Nanoscale

Accepted Manuscript

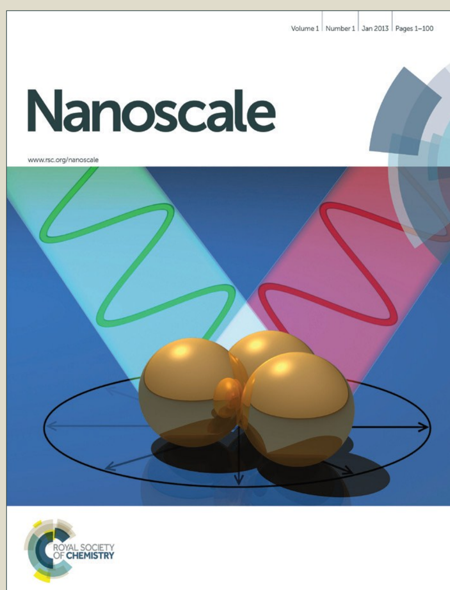

This is an *Accepted Manuscript*, which has been through the Royal Society of Chemistry peer review process and has been accepted for publication.

Accepted Manuscripts are published online shortly after acceptance, before technical editing, formatting and proof reading. Using this free service, authors can make their results available to the community, in citable form, before we publish the edited article. We will replace this *Accepted Manuscript* with the edited and formatted *Advance Article* as soon as it is available.

You can find more information about *Accepted Manuscripts* in the Information for Authors.

Please note that technical editing may introduce minor changes to the text and/or graphics, which may alter content. The journal's standard Terms & Conditions and the Ethical guidelines still apply. In no event shall the Royal Society of Chemistry be held responsible for any errors or omissions in this *Accepted Manuscript* or any consequences arising from the use of any information it contains.

ROYAL SOCIETY OF CHEMISTRY

www.rsc.org/nanoscale

Enhancing the electroluminescence efficiency of Si NCs/SiO_2 superlattice–based light-emitting diodes through hydrogen ion beam treatment

Sheng-Wen Fu, Hui-Ju Chen, Hsuan-Ta Wu, Shao-Ping Chen and Chuan-Feng Shih*

Department of Electrical Engineering, National Cheng Kung University, Tainan, 70101, Taiwan

*E-mail address: cfshih@mail.ncku.edu.tw

Abstract

This paper presents a novel method for enhancing the electroluminescence (EL) efficiency of ten-period silicon-rich oxide (SRO)/SiO_2 superlattice–based light-emitting diodes (LEDs). A hydrogen ion beam (HIB) was used to irradiate on each SRO layer of the superlattices to increase the interfacial roughness in nanoscale and density of the Si nanocrystals (Si NCs). Fowler–Nordheim (F–N) tunneling was the major mechanism for injecting the carriers into the Si NCs. The barrier height of the F–N tunneling was lowered by forming the nano-roughened interface and nonradiative P_b centers were passivated through the HIB treatment. Additionally, the reflectance of the LEDs was lowered because of the nano-roughened interface. These factors considerably increased the slope efficiency of EL and maximum output power of the LEDs. The lighting efficiency increased by an order of magnitude, and the turn-on voltage decreased considerably. This study established an efficient approach for obtaining bright Si NCs/SiO_2 superlattice-based LEDs.

Key words: hydrogen ion beam; silicon nanocrystals; nano-roughened; hydrogen passivation

Nanoscale Accepted Manuscript

Introduction

Since the discovery of strong room-temperature photoluminescence in nanoscale porous Si, Si nanocrystals (Si NCs) have attracted great attention because of their potential application in optoelectronic devices.[1-5] Enormous efforts have been paid to develop Si NC light-emitting diodes (Si NC LEDs) because that can be easily integrated with current complementary metal-oxide-semiconductor (CMOS) technology.[6-10] To this end, controlling of the size and nanostructure of Si NCs are regarded as the most important issues. It is known that when the size of Si NCs is smaller than the free exciton Bohr radius of bulk Si (approximately equal to 4.8 nm), the light emission efficiency can be drastically improved because of the increase in the overlapping of electron-hole wave functions; that is, quantum confinement effect (QCE).[11] However, when the size of Si NCs is only few nanometers, the surface and interface should hugely influence on the behaviors of Si NCs rather than the bulk that complicated the lighting behaviors of the Si NC LEDs.[12-14]

Silicon-rich oxide (SRO)/SiO_2 or silicon-rich nitride/SiO_2 superlattices-based LEDs have been widely investigated because their quantum efficiency (QE) is higher than randomly distributed Si NCs within dielectric matrix.[14-21] Nevertheless, a number of approaches have been recently developed to increase the QE, such as employing the field-effect,[7,22] introducing localized surface plasmons,[23-25] combination with hybrid organic,[26-28] replacing the SiO_x by SiN_x or SiC,[18,19,29,30] and passivation[31], etc. To date, external QE (EQE) of up to 2.4 % has been reported.[32] However, it is still insufficient for practical application.

The light emission mechanism of Si NCs embedded in dielectric matrix is mainly based on the radiative recombination occurring at surface radiative states surrounding the Si NCs and the band-to-band transition in Si NCs through QCE.[22-26,32-35] Moreover, the high refractive index differences exist between adjacent layers in the multilayered

Nanoscale Accepted Manuscript

structure devices (Si (n = 3.4), SiO_2 (n = 1.5), AZO (n = 3.3), and air (n = 1)), leading to a considerable Fresnel loss and total internal reflection at the heterojunction, which diminishes the light extraction efficiency. As a result, surface roughening is another effective way to improve the light extraction ratio by forming the anti-reflection surface and reducing the surface reflection.[23,36-38] However, the interface roughening between the SRO and the SiO_2 layers has not received much attention.

We have demonstrated in our previous study that subjecting an SRO layer to Ar ion beam treatment can increase the crystallinity and activate the defect emission that yields a spontaneous white photoluminescence in SRO/SiO_2 superlattices.[39] In the current study, the electroluminescence (EL) was efficiently increased and the operating voltage of Si NCs/SiO_2 superlattice-based LEDs was diminished by using a hydrogen ion beam (HIB) to treat the SRO layer. It was obtained that the HIB increased the nano-roughened interface and passivated the nonradiative centers, increasing the QE. The relationship between the nano-roughened interface and these factors that enhanced the EL were discussed.

Experimental details

Ten-period SRO/SiO_2 superlattices were sputtered on a p-type (100) Si wafer with a resistivity of 10–20 Ω-cm by repeating the following procedure: A 1.5 nm-thick SiO_2 layer was firstly deposited by the radio frequency (13.6 MHz) sputtering of a SiO_2 target; then a 1.5 nm-thick SRO layer was deposited by the DC sputtering of an intrinsic Si target, and the HIB was subsequently irradiated on the SRO surface by rotating the substrate. To avoid the possible contaminations, the targets were pre-sputtered for 5 min before the target shutter was opened to allow commencement of deposition. The power of the 3-in. SiO_2 target, 3-in. intrinsic Si target, and working pressure were 50 W, 90 W, and 0.8 mTorr, respectively. The anode

Nanoscale Accepted Manuscript

voltage of the HIB was used 0, 70 and 116 V, yielding an energy of 0, 70 and 116 eV, respectively. Ar gas was fed into a chamber at a flow rate of 12 sccm, and H_2 gas was introduced into the chamber through an end-hole gridless ion gun at a flow rate of 3 sccm. More information about this procedure was provided in our previous study.[39] All samples were subsequently annealed in a conventional quartz-tube furnace at 1,000 °C (10 ℃/ min) for 3 h under a pressure of 1 Torr with gas mixture (N_2 95% and H_2 5%). The thicknesses of the superlattices were determined through transmission electron microscopy (HR-TEM, JEOL/JEM-2100). Surface morphologies of SRO/SiO_2 fabricated using HIB with different energy levels were examined through atomic-force microscopy (AFM, Digital Instruments/Nanoscope E) in the tapping mode. The reflectance spectrum was obtained using a UV-VIS-NIR spectrometer (Hitachi/U-4100).

Regarding device fabrication, the active area was defined using a standard lithography process that etched the superlattices to form a circular mesa pattern, with an area of 1.6 mm^2, through an inductively coupled plasma technique. Moreover, 200-nm-thick aluminum-doped zinc oxide (AZO) was deposited on the superlattices as a transparent current spreading layer through sputtering. Finally, 1800-nm-thick Au films were deposited on the AZO and substrate backside as contacts through an electron-gun evaporator. The area of the top Au electrode fabricated through a lift-off process was 0.28 mm^2. The entire LED structure was Au/P-Si/$(SRO/SiO_2)_{10}$/AZO/Au, as shown in Fig. 1(a). Fig. 1(b) depicts the LED operated at a forward current of 216 mA and operating voltages of 25.5 V by using a digital photographic camera with an exposure time of 1 s.

All the device properties were measured at room temperature. Current–voltage (I–V) characteristics of the devices were measured through Keithley 2400 using forward bias. A positive voltage was applied to the Au electrode on the p-type

Nanoscale Accepted Manuscript

substrate. The Si-based LED was placed on a flat stage with a cooling system maintained at 25 ℃. The EL spectrum was measured using a monochromator (Zolix/omni-λ3008) combined with a photomultiplier tube (PMT, Zolix/PMTH-S1-CR131).

Results and discussion

Fig. 2 shows the HR-TEM cross-section images of the SRO/SiO_2 structure. Ten-period superlattices with clear interfaces were observed. The thicknesses of SRO and SiO_2 were approximately 1.5 (dark region) and 1.5 nm (grey region), respectively. For the reference sample (Fig. 2(a), 0-eV HIB treatment), no crystalline Si NCs were observed. This observation is consistent with that of Zacharias *et al.*,[40] who reported that fabricating Si NCs within a SRO layer with a thickness less than 1.6 nm was difficult because an extremely high Gibbs free energy was introduced during the formation of Si NCs by increasing the amount of amorphous/crystalline Si and oxide/crystalline Si interfaces. In addition, the thickness of SiO_2 was less than 2 nm, and therefore, the nucleation of the Si NCs was difficult. It was because the formation of a rough SiO_2/SRO interface reduced the driving forces of the self-assembled Si NCs.[41] Despite these limitations, crystalline Si NCs were obtained in the 116-eV sample, as shown in the inset of Fig. 2(b). The size of the Si NCs was approximately 1.6 nm, and the thickness of SiO_2 was approximately 1.5 nm. A thin SiO_2 layer was deliberately designed to lower the turn-on voltage of the LEDs by increasing the tunneling probability. Using the HIB facilitated forming the Si NCs between the thin SiO_2 layers. It should be mentioned that not all Si NCs could be observed by TEM when their size was smaller than ~1 nm. Actually, these NCs also contribute to the lighting and carrier transport. Their lattice images can only be observed when they are oriented in the same way as the substrate orientation, as the electron beam is aligned

Nanoscale Accepted Manuscript

to the substrate zone axis (c-Si (111) plane).[41,42,43,44] Hence, the total proportion of the Si NCs inside the SRO layers was actually much higher than the visible Si NCs in the TEM images, as shown by Yurtsever *et al.*[45] through direct comparison of TEM and plasmon tomography. Therefore, the interfaces of the SRO and SiO_2 layers became wavy because of the formation of fine Si NCs in the 116-eV sample, as shown in Fig. 2(b). This fact suggested that the formation of Si NCs in the ultra-thin 1.5-nm-SRO layers also changed the interfacial morphology in nanoscale.

To estimate the influence of the HIB on the interfacial morphology, the surface morphologies of the SRO/SiO_2 superlattices prepared using HIB-assisted sputtering were revealed through AFM. Figs. 3 (a), (b), and (c) show 1 μm × 1 μm (20-nm data scale) images of the samples prepared using HIB energies of 0, 70, and 116 eV, respectively. The surface roughness increased with the HIB energy. The root-mean-square (rms) roughness of the reference sample (0 eV) was only 0.2 nm. By contrast, the rms roughness values of the other two samples (70 and 116 eV; Figs. 3(b) and (c) were 0.5 and 0.8 nm, respectively. An increase in the roughness was ascribed to the formation of Si NCs.[39] Moreover, in our superlattice structure, the thicknesses of the SRO and SiO_2 layers were as low as approximately 1.5 nm. The variation in rms roughness from 0.2 to 0.8 nm was approximately 26%. Such a marked variation is not a common surface phenomenon, thus implying that the interface between the SRO and SiO_2 layers also roughens. This observation is consistent with the results in the TEM images (Fig. 2).

To determinate the characteristic of the HIB on the electrical properties of Si NCs/SiO_2 superlattice-based LEDs, the carrier transport behaviors were characterized according to I–V relationship, as shown in Fig. 4. When a forward bias was applied, the electrons and holes were injected from the p-type substrate and Au electrode into the superlattices, respectively. The tunneling probability was strongly associated with

Nanoscale Accepted Manuscript

the density of Si NCs and thickness of the SiO_2 layer. Because the thickness of the SiO_2 layer was the same in all of our samples, the current density was directly related to the density of the Si NCs. Fig. 4(a) illustrates the I–V characteristics. As expected, when the ion-beam energy increased from 0 to 116 eV, the tunneling current was enhanced, consequently minimizing the turn-on voltage from 14.8 to 6 V. It should be noted that the slope of the injection current versus voltage curve of the 70-eV sample declined when the voltage exceeded 22 V. This phenomenon was ascribed to that the HIB increased the current through preferential conductive paths. An increase in the injection current also introduced joule heating that decreased the carrier transport efficiency. This effect was relaxed by further increasing the HIB energy to 116 eV because more conducting channels were formed. Moreover, to determine the carrier transport mechanism, the current density (J) and electric field (E) were determined according to the current and voltage and were used for analyzing the transport mechanism. The Fowler–Nordheim (F–N) equation is expressed as[46-48]

$$J_{FN} = \frac{A}{4\phi_B} E^2 e^{-\frac{2B\phi_B^{3/2}}{3E}} \quad (1)$$

where A and B are constants, ϕ_B is an effective barrier height for carrier injection, and E is the electric field; ϕ_B can be evaluated using the slope of the linear region of the F–N plots, as shown in Fig. 4(b). A linear relation in the high-field side clearly revealed that the major tunneling mechanism was the F–N tunneling. When the ion-beam energy increased from 0 to 116 eV, the threshold field decreased from 3.2 to 2 MV/cm and the effective barrier height decreased from 2.1 to 0.8 eV. A decrease in the turn-on voltage, threshold voltage, and effective barrier height corresponded to an increase in the HIB energy and rms roughness. These relationships are plotted in Fig. 4(c). Lin *et al.*[49] reported that the threshold field of the F–N tunneling was minimized when Si was fabricated in nanopyramids, which increased the field enhancement

Nanoscale Accepted Manuscript

effect near the pyramid tip. In the current study, the field enhancement factor was increased by roughening the SiO_2/SRO interface through the HIB. The schematic illustrations were shown in Figs. 5(a)-(c). The number of Si NCs increased with HIB energy and the interface became nano-roughened. Because the interface roughens through HIB, the carriers accumulate around the sharp edge of the interface and cross the SiO_2 barriers easily, leading to the formation of a number of preferential conductive paths and thus a reduction in the effective barrier height. Moreover, an increase in the density of the Si NCs resulted in an increasing interaction of the carrier wave functions and shortened the tunneling distance. Therefore, the current density was increased and threshold field was diminished. Accordingly, we suggest that the HIB-induced increase in nano-roughened interface effectively facilitates the process of reducing the turn-on voltage and effective barrier height.

To understand the effect of the HIB on the EL properties of Si NC/SiO_2 superlattices-based LEDs, EL spectra of the devices with various HIB energies were measured. Figs. 6 (a)–(c) show the power-dependent EL spectra of the Si NCs/SiO_2 superlattice–based LEDs. The EL peak was resolved using two sub-peaks located at 520 and 650 nm. These peaks originated from the radiative recombination at the Si NCs surface and band-to-band transition within the Si NCs because of QCE, respectively.[22-26,32-35] The EL peak intensity (I_{EL}) increased with the injection current. Moreover, I_{EL} was significantly enhanced when the ion-beam energy was increased from 0 to 116 eV. The I_{EL} values of the devices fabricated using 70-eV and 116-eV HIB increased by 4 and 7 times, respectively, compared with those of the reference device (0 eV) at the same injection current of 72 mA. This suggested that the enhancement of QE was achieved by increasing the HIB energy. The saturation current was doubled for the 116-eV device compared with that of the reference device.

Nanoscale Accepted Manuscript

Fig. 7(a) shows plots of the ratios of the integrated I_{EL} as a function of the input power. The slope (dashed line) represents the EL efficiency. Because the input power was less than 3 W, the EL efficiency of the 70-eV and 116-eV HIB treated samples increased by 3.6 and 11 times, respectively, compared with those of the reference device (0-eV). The enhancement of the EL intensity by using the HIB was as expected because the increase in the tunneling probability and carrier density enhanced the radiative recombination rate. Fig. 7(b) illustrates plots of the ratios of the integrated I_{EL} to the injected current density, which reflect the EQE, as a function of the input power. The devices fabricated using 0-eV and 70-eV HIBs achieved the maximum output power level when the input power was 2–3 W, whereas the device fabricated using 116-eV HIB achieved the maximum output power level for an input power of up to 4.2 W. A drop in the EQE indicated carrier overflow and the Auger nonradiative recombination process was occurred.[14,50,51] A considerably enhanced EL power efficiency of the Si NC/SiO_2 superlattices-based LEDs was achieved by employing HIB.

Another possible mechanism that enhances the EL intensity is the reduction in reflectance. Because the considerable difference in the refractive indices of SRO (3.4–1.5) and SiO_2 (1.5), the emission light is internally reflected in the interface according to Snell's law. This suggests that only a few portion of the emission light can escape from the multilayered structure, resulting in extremely low EQE. Therefore, a roughened interface that can serve as an intermediate medium with a gradient refractive index, which enables eliminating the internal reflection that induces light trapping and increasing the light extraction efficiency, is required.[52] This concept has been extensively applied to GaN-based LEDs, such as those grown on patterned substrates, and for roughening p-GaN.[53] Fig. 8 illustrates the reflectance spectrum for the SRO/SiO_2 superlattices. In the visible region, the reflectance decreased markedly

Nanoscale Accepted Manuscript

from approximately 40% to 18% when the ion energy increased from 0 to 116 eV, indicating that the roughened interface eliminated the reflection of light in the periodic interfaces between the SRO and SiO_2 layers.

Hydrogen passivation[54] during the HIB treatment improves radiative recombination. Fig. 9 shows electron spin resonance (ESR) spectra, which were measured at room temperature, of the samples with various HIB energy levels. The zero-crossing of the first derivative was clearly identifiable at g-factor 2.005 for the samples fabricated using 0-eV and 70-eV HIBs, which corresponds to the characteristic signature of the P_b center.[55,56] This center is produced through Si dangling bonds located at the Si NCs–SiO_2 interface, which is a nonradiative recombination center that quenches the luminescence, irrespective of whether the source originated from the quantum confinement or surface states.[57] The peak at g-factor 2.005 did not appear in the ESR spectrum of the device fabricated using a 116-eV HIB, clearly indicating that the availability of HIB with this energy scale passivates the dangling bonds at the interface. Therefore, light emission is enhanced by eliminating the number of dangling bonds, minimizing the nonradiative recombination.

Conclusions

We demonstrate a high-efficiency visible Si NCs/SiO_2 superlattice-based LEDs by employing the HIB. The nano-roughened interface and density of Si NCs increased. The F–N tunneling was the major mechanism for injecting carriers into the Si NCs. The barrier height of the F–N tunneling was lowered and the nonradiative recombination centers, such as P_b centers, were passivated through the HIB treatment. These two factors increased the slope efficiency of EL and maximum output power of the LEDs. The lighting efficiency increased by an order of magnitude, and the turn-on

Nanoscale Accepted Manuscript

voltage markedly decreased. The HIB treatment is an efficient method for obtaining high-efficiency Si NC–based LEDs in the future.

Acknowledgments

The authors thank the Ministry of Science and Technology, Taiwan, for financially supporting this study under Contract No. MOST 102-2221-E-006-238 -MY3.

Nanoscale Accepted Manuscript

Reference

1. L. T. Canham, *Appl. Phys. Lett.*, 1990, **57**, 1046-1048.
2. A. G. Cullis and L. T. Canham, *Nature*, 1991, **353**, 335-338.
3. L. Pavesi, L. Dal Negro, C. Mazzoleni, G. Franzo and F. Priolo, *Nature*, 2000, **408**, 440-444.
4. L. Fan, J. Wang, L. T. Varghese, H. Shen, B. Niu, Y. Xuan, A. M. Weiner and M. Qi, *Science*, 2012, **335**, 447-450.
5. F. Priolo, T. Gregorkiewicz, M. Galli and T. F. Krauss, *Nat Nano*, 2014, **9**, 19-32.
6. N.-M. Park, T.-S. Kim and S.-J. Park, *Appl. Phys. Lett.*, 2001, **78**, 2575.
7. R. J. Walters, G. I. Bourianoff and H. A. Atwater, *Nature Materials*, 2005, **4**, 143-146.
8. J.-M. Shieh, Y.-F. Lai, W.-X. Ni, H.-C. Kuo, C.-Y. Fang, J. Y. Huang and C.-L. Pan, *Appl. Phys. Lett.*, 2007, **90**, 051105.
9. J. A. Luna-López, A. Morales-Sánchez, M. Aceves-Mijares, Z. Yu and C. Domínguez, *J. Vac. Sci. Technol. A*, 2009, **27**, 57-62.
10. T. Hung-Yu, C. Chih-Hsien and L. Gong-Ru, *Selected Topics in Quantum Electronics, IEEE Journal of*, 2014, **20**, 218-224.
11. S. V. Gaponenko, *Optical Properties of Semiconductor Nanocrystals*, Cambridge University Press, 1998.
12. L. Palacios-Huerta, S. A. Cabanas-Tay, J. A. Luna-Lopez, M. Aceves-Mijares, A. Coyopol and A. Morales-Sanchez, *Nanotechnology*, 2015, **26**, 395202.
13. S. A. Cabañas-Tay, L. Palacios-Huerta, J. A. Luna-López, M. Aceves-Mijares, S. Alcántara-Iniesta, S. A. Pérez-García and A. Morales-Sánchez, *Semicond. Sci. Technol.*, 2015, **30**, 065009.
14. J. López-Vidrier, Y. Berencén, S. Hernández, B. Mundet, S. Gutsch, J. Laube, D. Hiller, P. Löper, M. Schnabel, S. Janz, M. Zacharias and B. Garrido, *Nanotechnology*, 2015, **26**, 185704.
15. Z. H. Lu, D. J. Lockwood and J. M. Baribeau, *Nature*, 1995, **378**, 258-260.
16. C. L. Heng, Y. Chen, Z. C. Ma, W. H. Zong and G. G. Qin, *J. Appl. Phys.*, 2001, **89**, 5682-5686.
17. A. Anopchenko, A. Marconi, M. Wang, G. Pucker, P. Bellutti and L. Pavesi, *Appl. Phys. Lett.*, 2011, **99**, -.
18. C. Huh, K. H. Kim, B. K. Kim, W. Kim, H. Ko, C. J. Choi and G. Y. Sung, *Adv. Mater.*, 2010, **22**, 5058-5062.
19. G.-R. Lin, Y.-H. Pai, C.-T. Lin and C.-C. Chen, *Appl. Phys. Lett.*, 2010, **96**, -.
20. L. Ding, M. B. Yu, X. Tu, G. Q. Lo, S. Tripathy and T. P. Chen, *Optics Express*, 2011, **19**, 2729-2738.

Nanoscale Accepted Manuscript

21. D. Di, I. Perez-Wurfl, L. Wu, Y. Huang, A. Marconi, A. Tengattini, A. Anopchenko, L. Pavesi and G. Conibeer, *Appl. Phys. Lett.*, 2011, **99**, 251113.
22. J.-R. Chen, D.-C. Wang, H.-C. Hao and M. Lu, *Appl. Phys. Lett.*, 2014, **104**, 061105.
23. W. Li, S. Wang, M. Hu, S. He, P. Ge, J. Wang, Y. Y. Guo and L. Zhaowei, *Sci. Rep.*, 2015, **5**.
24. C. Jia-Rong, Z. Zhi-Quan, H. Hong-Chen and L. Ming, *Nanotechnology*, 2014, **25**, 355203.
25. D. Li, F. Wang and D. Yang, *Nanoscale*, 2013, **5**, 3435-3440.
26. F. Maier-Flaig, J. Rinck, M. Stephan, T. Bocksrocker, M. Bruns, C. Kubel, A. K. Powell, G. A. Ozin and U. Lemmer, *Nano letters*, 2013, **13**, 475-480.
27. D. P. Puzzo, E. J. Henderson, M. G. Helander, Z. Wang, G. A. Ozin and Z. Lu, *Nano letters*, 2011, **11**, 1585-1590.
28. Z. Yang, M. Dasog, A. R. Dobbie, R. Lockwood, Y. Zhi, A. Meldrum and J. G. C. Veinot, *Adv. Funct. Mater.*, 2014, **24**, 1345-1353.
29. X. Wang, R. Huang, C. Song, Y. Guo and J. Song, *Appl. Phys. Lett.*, 2013, **102**, 081114.
30. C. Huh, T.-Y. Kim, C.-G. Ahn and B. K. Kim, *Appl. Phys. Lett.*, 2015, **106**, 211103.
31. B. Puthen Veettil, L. Wu, X. Jia, Z. Lin, T. Zhang, T. Yang, C. Johnson, D. McCamey, G. Conibeer and I. Perez-Würfl, *Appl. Phys. Lett.*, 2014, **105**, 222108.
32. C.-H. Cheng, Y.-C. Lien, C.-L. Wu and G.-R. Lin, *Optics Express*, 2013, **21**, 391-403.
33. G.-R. Lin, C.-J. Lin, C.-K. Lin, L.-J. Chou and Y.-L. Chueh, *J. Appl. Phys.*, 2005, **97**, 094306.
34. D. Y. Chen, D. Y. Wei, J. Xu, P. G. Han, X. Wang, Z. Y. Ma, K. J. Chen, W. H. Shi and Q. M. Wang, *Semicond. Sci. Technol.*, 2008, **23**, 015013.
35. K.-Y. Cheng, R. Anthony, U. R. Kortshagen and R. J. Holmes, *Nano letters*, 2011, **11**, 1952-1956.
36. Y. Liu, J. Xu, H. Sun, S. Sun, W. Xu, L. Xu and K. Chen, *Optics Express*, 2011, **19**, 3347-3352.
37. Y. Guo, Z. Lin, R. Huang, Z. Lin, C. Song, J. Song and X. Wang, *Opt. Mater. Express*, 2015, **5**, 969-976.
38. C. Huh, B. K. Kim, C.-G. Ahn, C.-J. Choi and S.-H. Kim, *Appl. Phys. Lett.*, 2014, **105**, 031108.
39. C.-F. Shih, C.-Y. Hsiao and K.-W. Su, *Optics Express*, 2013, **21**, 15888-15895.
40. M. Zacharias and P. Streitenberger, *Phys. Rev. B*, 2000, **62**, 8391-8396.

Nanoscale Accepted Manuscript

41. M. Zacharias, J. Heitmann, R. Scholz, U. Kahler, M. Schmidt and J. Bläsing, *Appl. Phys. Lett.*, 2002, **80**, 661-663.
42. T. C.-J. Yang, Y. Kauffmann, L. Wu, Z. Lin, X. Jia, B. Puthen-Veettil, T. Zhang, G. Conibeer, I. Perez-Wurfl and A. Rothschild, *Appl. Phys. Lett.*, 2014, **105**, 053116.
43. C. R. Perrey, S. Thompson, M. Lentzen, U. Kortshagen and C. B. Carter, *J. Non-Cryst. Solids*, 2004, **343**, 78-84.
44. G. Conibeer, M. Green, R. Corkish, Y. Cho, E.-C. Cho, C.-W. Jiang, T. Fangsuwannarak, E. Pink, Y. Huang, T. Puzzer, T. Trupke, B. Richards, A. Shalav and K.-l. Lin, *Thin Solid Films*, 2006, **511–512**, 654-662.
45. A. Yurtsever, M. Weyland and D. A. Muller, *Appl. Phys. Lett.*, 2006, **89**, 151920.
46. R. H. Fowler and L. Nordheim, 1928.
47. Z. A. Weinberg, *J. Appl. Phys.*, 1982, **53**, 5052-5056.
48. D. K. Schroder, *Semiconductor material and device characterization*, John Wiley & Sons, 2006.
49. G.-R. Lin, C.-J. Lin and C.-K. Lin, *Optics express*, 2007, **15**, 2555-2563.
50. S. K. Ray, S. Maikap, W. Banerjee and S. Das, *J. Phys. D: Appl. Phys.*, 2013, **46**, 153001.
51. B. Ghosh, Y. Masuda, Y. Wakayama, Y. Imanaka, J.-i. Inoue, K. Hashi, K. Deguchi, H. Yamada, Y. Sakka, S. Ohki, T. Shimizu and N. Shirahata, *Adv. Funct. Mater.*, 2014, **24**, 7151-7160.
52. J. J. Wierer, A. David and M. M. Megens, *Nat Photon*, 2009, **3**, 163-169.
53. H. Hung-Wen, J. T. Chu, C. C. Kao, T. H. Hseuh, T. C. Lu, H. C. Kuo, S. C. Wang and C. C. Yu, *Nanotechnology*, 2005, **16**, 1844.
54. B. G. Lee, D. Hiller, J.-W. Luo, O. E. Semonin, M. C. Beard, M. Zacharias and P. Stradins, *Adv. Funct. Mater.*, 2012, **22**, 3223-3232.
55. S. P. Withrow, C. W. White, A. Meldrum, J. D. Budai, D. M. Hembree and J. C. Barbour, *J. Appl. Phys.*, 1999, **86**, 396-401.
56. B. Garrido Fernandez, M. López, C. García, A. Pérez-Rodríguez, J. R. Morante, C. Bonafos, M. Carrada and A. Claverie, *J. Appl. Phys.*, 2002, **91**, 798-807.
57. S. Godefroo, M. Hayne, M. Jivanescu, A. Stesmans, M. Zacharias, O. I. Lebedev, G. Van Tendeloo and V. V. Moshchalkov, *Nature nanotechnology*, 2008, **3**, 174-178.

Nanoscale Accepted Manuscript

Figure captions

Fig. 1 (a) Schematic of the SRO/SiO_2 superlattice-based LED structure and (b) image of the LED emission obtained at an energy of 116 eV, forward current of 216 mA, and a bias of 25.5 V.

Fig. 2 HR-TEM micrographs of SRO/SiO_2-superlattice structures fabricated using HIBs with energies of (a) 0 eV and (b) 116 eV. The inset illustrates the formation of Si NCs with size less than 2 nm by using an HIB with energy of 116 eV.

Fig. 3 AFM images of SRO/SiO_2 superlattices prepared by employing HIB with (a) 0, (b) 70, and (c) 116 eV.

Fig. 4 (a) I–V curves and (b) the plots of $\ln(I/E^2)$ as a function of 1/E for the Si NCs/SiO_2 superlattice-based LEDs at various HIB energies from 0 to 116 eV. (c) The threshold F–N tunneling electric field, turn-on voltage and effective barrier height as a function of the HIB energy and rms roughness.

Fig. 5 Schematic of the variation of the SRO/SiO_2 interface induced by employing HIB with (d) 0, (e) 70, and (f) 116 eV. The gray and blue patterns represent the SRO and SiO_2 layers, respectively, and the blue dot represents the Si NCs. As the HIB energy increases, the number of Si NCs increase more and nanoscale interface becomes nano-roughened.

Fig. 6 EL spectra of the Si NCs/SiO_2 superlattice-based LEDs fabricated with HIB energies of (a) 0, (b) 70, and (c) 116 eV as a function of the injection current measured at room temperature.

Nanoscale Accepted Manuscript

Fig. 7 (a) Integrated I_{EL} and (b) ratio of the integrated I_{EL}/current (EQE) as a function of input power.

Fig. 8 Reflection spectra of the SRO/SiO_2 superlattices at various HIB energies (rms roughness).

Fig. 9 ESR spectra of the SRO/SiO_2 superlattices at various HIB energies.

Nanoscale Accepted Manuscript

Fig. 1

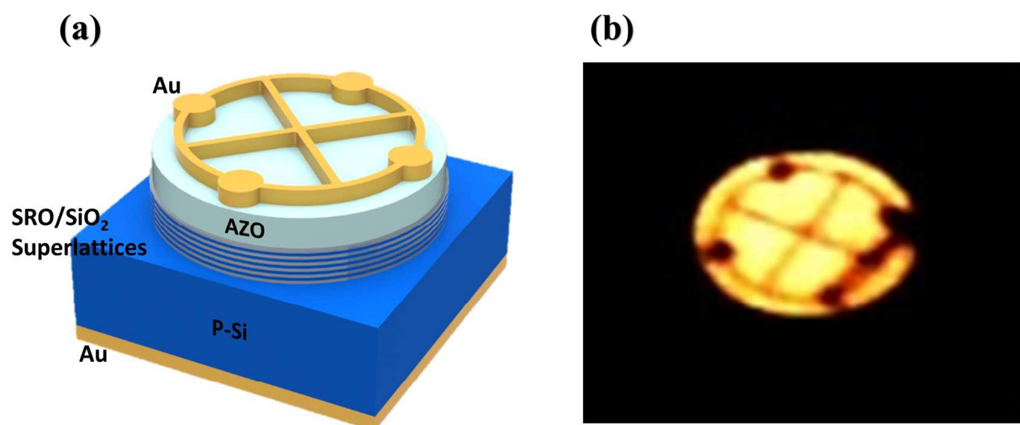

Fig. 2

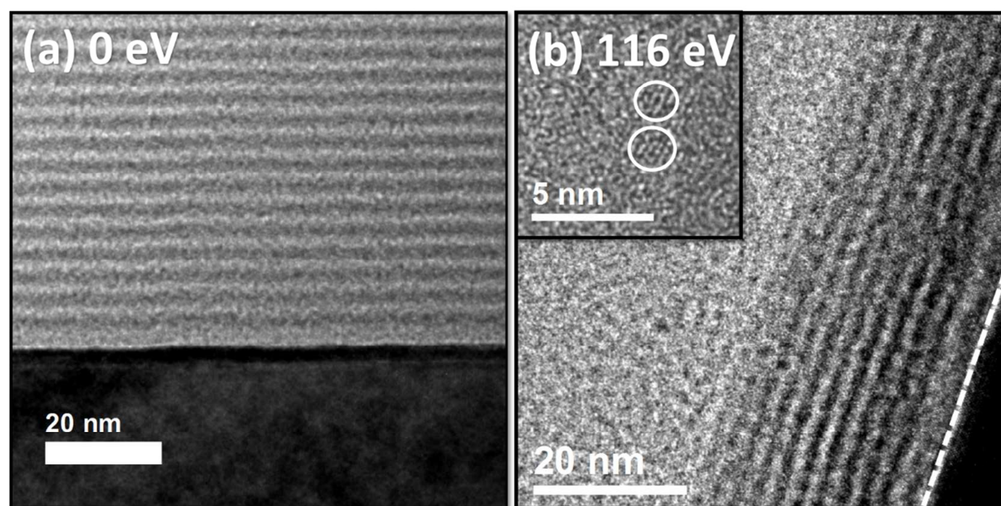

Fig. 3

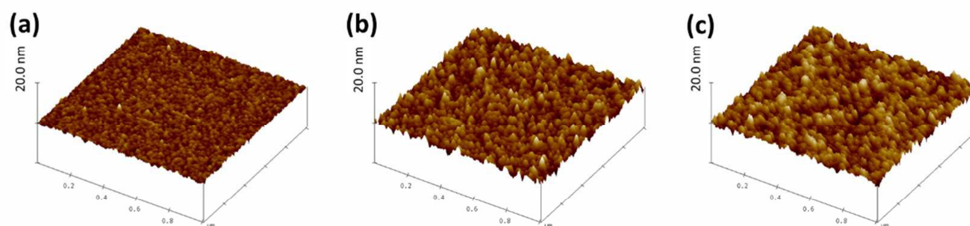

Nanoscale Accepted Manuscript

Fig. 4

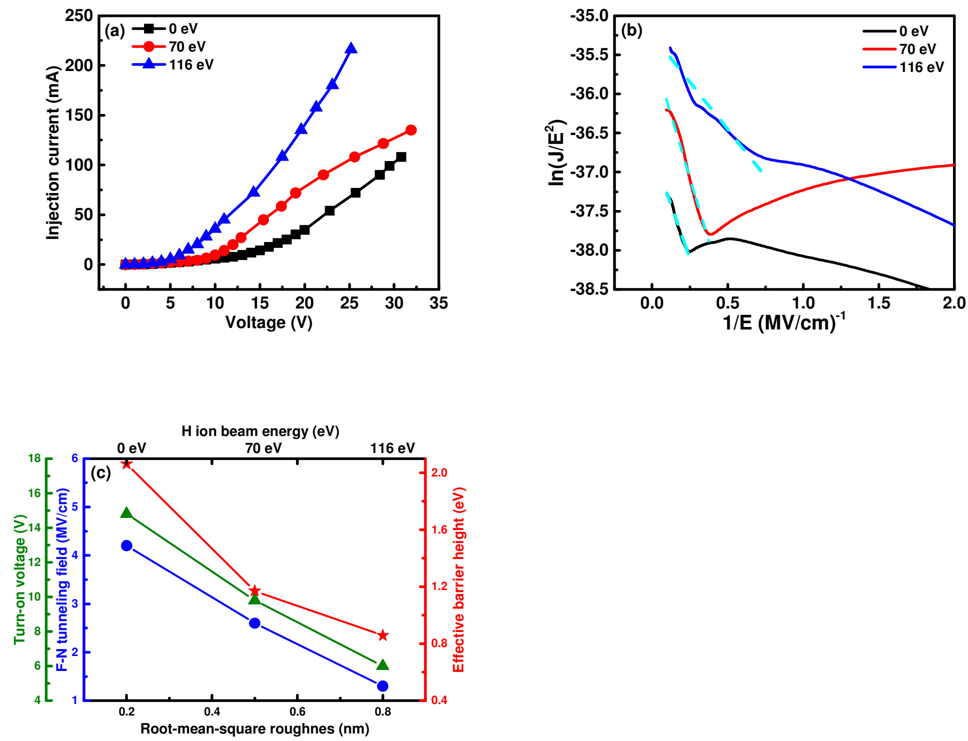

Fig. 5

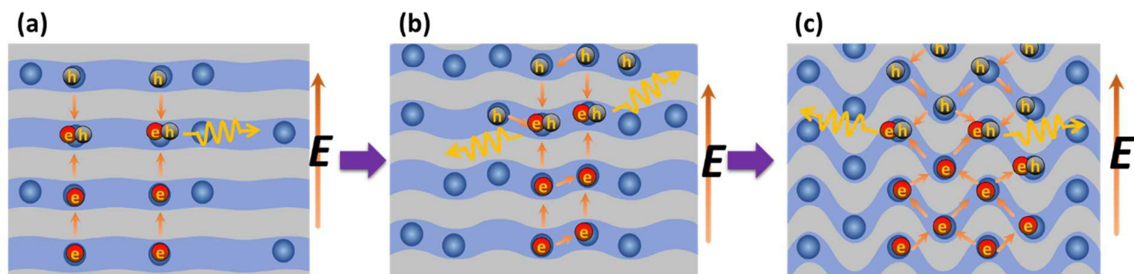

Nanoscale Accepted Manuscript

Fig. 6

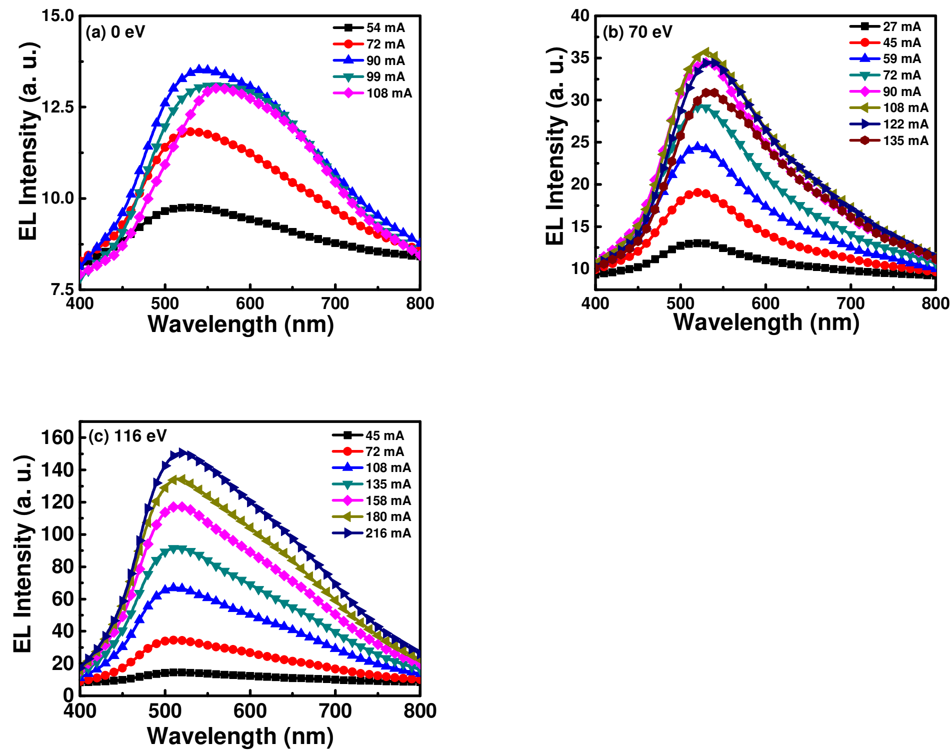

Fig. 7

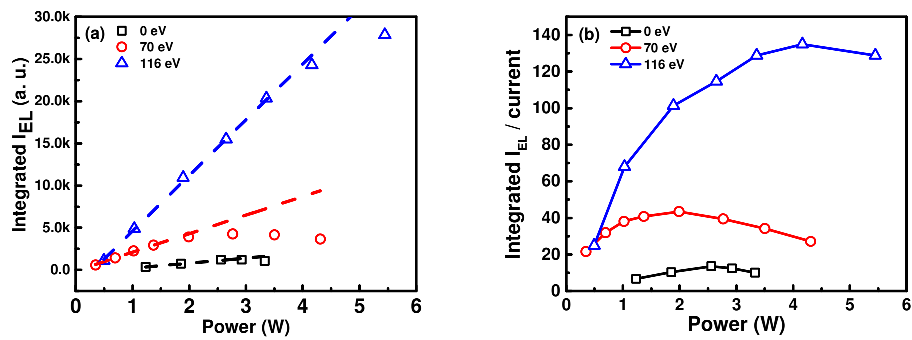

Nanoscale Accepted Manuscript

Fig. 8

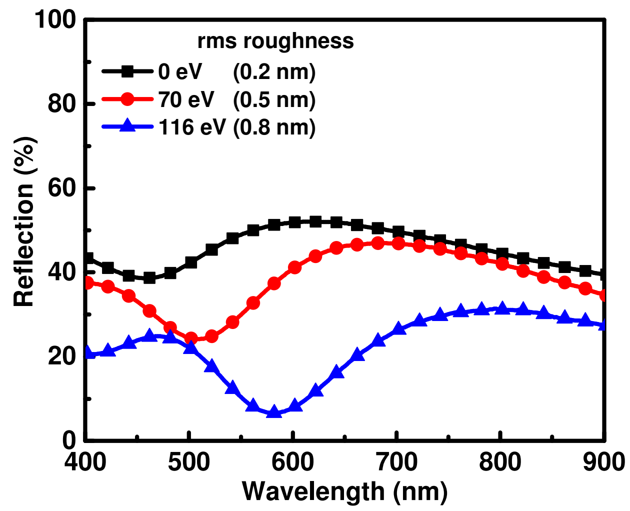

Fig. 9

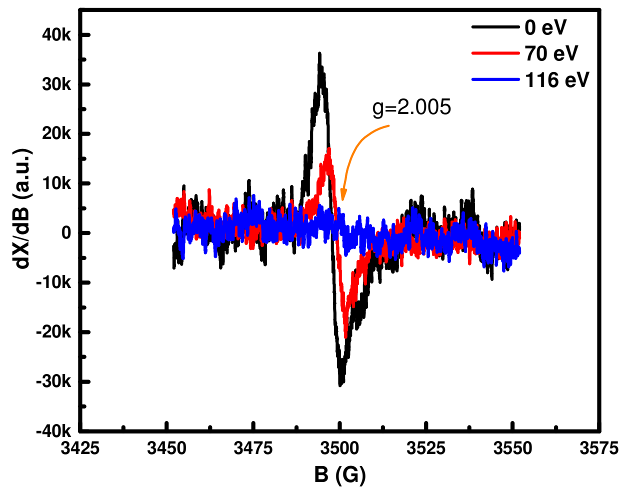

Nanoscale Accepted Manuscript